Int. J. Electrochem. Sci., 16**(2021)** Article ID: 210910, doi: 10.20964/2021.09.10

International Journal of ELECTROCHEMICAL SCIENCE
www.electrochemsci.org

Detection of Chrysin as Agent for potential treatment of Alzheimer's Disease using Electrochemical sensor Based on CuO@Ta_2O_5 nanocomposite Modified Glassy Carbon Electrode

Lin Fu[1], *Xuexia Wang*[2,*]

[1] Plastic Surgery For External Burn, Yidu Central Hospital of Weifang, Qingzhou, 262500, China
[2] School of Nursing, Shandong University of Traditional Chinese Medicine, Ji'nan, 250355, China
[*]E-mail: wangxuexia0813@163.com, XuexiaWang@protonmail.com

Received: 3 May 2021/ *Accepted:* 17 June 2021 / *Published:* 10 August 2021

In this work, the CuO@Ta_2O_5 nanocomposite was synthesized, and the chemical stability and sensing capabilities of the CuO@Ta_2O_5 nanocomposite as a chrysin sensor were improved. The nanocomposite was electrodeposited on a glassy carbon electrode (GCE), and structural analyses using SEM and XRD indicated that the GCE was uniformly coated with high porosity CuO@Ta_2O_5 nanoparticles. The amperometry and cyclic voltammetry experiments showed the high sensitive, selective, stable and accurate response of CuO@Ta_2O_5/GCE to chrysin determination because of the formation of a hetero-interface between CuO and Ta_2O_5 nanostructures, which facilitates charge migration and enhances the catalytic activity of CuO@Ta_2O_5/GCE. Results showed that the linear range, detection limit and sensitivity were obtained at 10 to 100µM, 0.008µM and 0.92921µA/µM, respectively. The practicality of the proposed electrochemical sensor in real samples was studied and results indicated the obtained recovery (96.00% to 98.00%) and RSD (2.77% to 3.11%) values were acceptable, illustrating that CuO@Ta_2O_5/GCE can be used as a practical sensor to detect chrysin in pharmaceutical and biological samples.

Keywords: Chrysin; Electrochemical sensor; Nanocomposite; Amperometry; Voltammetry

1. INTRODUCTION

Chrysin (5,7-Dihydroxy-2-phenyl-4H-1-benzopyran-4-one) is a hydroxylated flavone found in honey, bee propolis, and various plants such as carrots, mushrooms, passion flowers, Passifloracaerulea, Pelargonium crispum, Passifloraincarnata and Oroxylumindicum [1, 2]. Studies have shown chrysin can act as a promising anticancer and phytochemical agent for the treatment of various neurodegenerative disorders such as Parkinson, Alzheimer, Huntington, amyotrophic lateral sclerosis and multiple sclerosis [3, 4].

Many studies have indicated inhibitory, anti-inflammatory functions and cytotoxic activities of chrysin on hepatocellular, breast, prostate and pancreatic carcinoma adenocarcinoma cells [5, 6]. Chrysin can help to improve memory in older adults through attenuating the increase in reactive species levels and the inhibition of the activities of superoxide dismutase, catalase and glutathione peroxidase [7, 8]. This flavonoid, as an antioxidant compound, also protects against hippocampal neuronal cell damage by free radical scavenger action [9, 10]. Therefore, chrysin has been widely used in dietary supplements and pharmaceutical applications.

Accordingly, many researchers have been focused on the synthesis, extracting and determination of chrysin in plants and medications [11-15]. Studies have indicated that identification and determination of chrysin levels has been conducted using liquid chromatography tandem mass spectrometry (LC–MS/MS), ultra-performance liquid chromatography–tandem mass spectrometry (UPLC–MS/MS), and electrochemical techniques such as cyclic voltammetry (CV), linear sweep voltammetry (LSV) and square wave voltammetry (SWV) [16, 17]. Electrochemical techniques are among the most effective, low-cost, and fast-responding methods for determining flavones in pharmaceutical and biological samples [18, 19]. For example, Xie et al. [11, 20] modified the carbon paste electrodes by activating Ta_2O_5 particles and Ta_2O_5-chitosan composite, and showed that the prepared electrochemical chrysin sensors were selective. There have been few studies into the stability, high sensitivity, and wide range of chrysin sensors. Therefore, this study was carried out for the synthesis of CuO@Ta_2O_5 nanocomposite and improvement of chemical stability and enhancement of sensing properties of CuO@Ta_2O_5 nanocomposite as a chrysin sensor.

2. EXPERIMENTAL

The electrodeposition method was applied for modification of GCE by a nanocomposite of CuO@Ta_2O_5 [21]. First, to obtain a mirror-like surface of GCE, the GCE surface was successively polished on a fine micro cloth with 0.3 µm and 0.05 µm alumina slurries (99%, Dongguan Yutian New Materials Co., Ltd., China) for 10 minutes, respectively. The polished electrode was washed with deionized (DI) water and ethanol (99%, Shandong Aojin Chemical Technology Co., Ltd., China) after each polishing step. Then, the electrodeposition electrolyte was prepared from 1mM $TaCl_5$ (99.99%, Sigma-Aldrich) and 1mM $CuCl_2$ (99.99%, Sigma-Aldrich) which were ultrasonically dissolved in an equal volume ratio of a mixture of DI water and 0.1mM HCl (33%, Qingdao Hot Chemicals Co., Ltd., China) at 45°C for 20 minutes. Electrodeposition and all electrochemical measurements were performed in a system Autolab PGSTAT 30 (Eco Chemie, Metrohm, Autolab B.V., Utrecht, The Netherlands) containing three-electrode cell using a platinum wire as auxiliary, GCE as working, and Ag/AgCl as reference electrodes. Electrodeposition was conducted at an applied voltage of -0.8 V to +0.7 V at a scan rate of 15mV/s for 20 minutes under magnetic stirring at 45°C.

Amperometric and CV measurements were performed in 0.1 M phosphate buffer solutions (PBS), which were prepared from H_3PO_4 (85%, Shandong Baovi Energy Technology Co., Ltd., China) and NaH_2PO_4 (99%, Merck, Germany) at pH 7.5. In order to prepare the real sample, the chrysin capsules were purchased from a local pharmacy. The powder of the capsules was extracted and

ultrasonically dissolved in 0.1M PBS at pH 7.5 at 40 °C for 45 minutes. The obtained suspension was filtered and stored in the refrigerator at 4 °C for amperometric measurements on CuO@Ta2O5/GCE under successive addition of chrysin solution with a rotation speed of 1000 rpm at 0.43 V. For determination of chrysin content in capsules, high performance liquid chromatography (HPLC, Tianjin Kermel Chemical Reagent Co. Ltd., China) was also employed for comparison between the obtained results. The analytical study was performed by a standard addition method.

Scanning electron microscopy and X-ray diffraction (XRD; D5005, Siemens AG, Munich, Germany) with 1.5404 Å (Cu Kα) were applied for morphological and structural analyses of electrodeposited samples.

3. RESULTS AND DISCUSSION

3.1 Morphological and structural analyses of electrodeposited samples

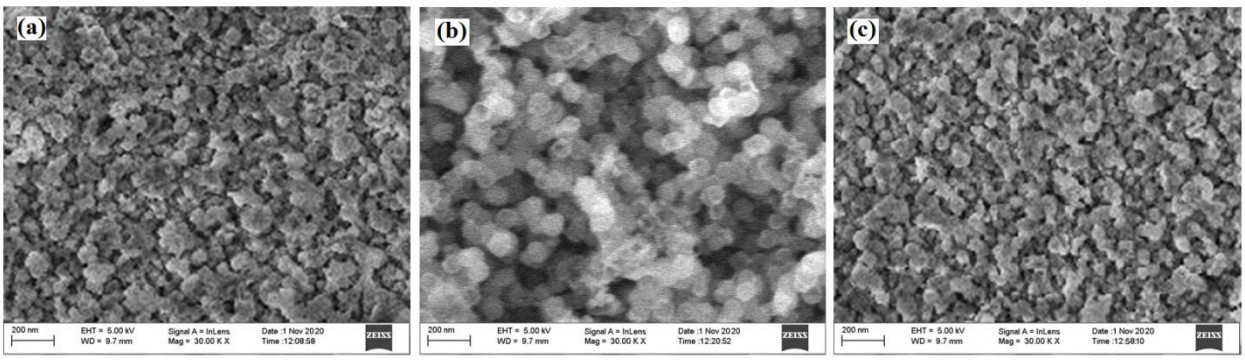

Figure 1. SEM images of electrodeposited CuO, Ta_2O_5 and CuO@Ta_2O_5 nanocompositeon GCE.

SEM images of electrodeposited CuO, Ta_2O_5 and CuO@Ta_2O_5 nanocomposite on GCE are shown in Figure 1. Figure 1a displays the formation of CuO nanoparticles with an average size of 60 nm, which indicates appropriate homogeneity, good separation and a spherical shape. The SEM image of Ta_2O_5 in Figure 1b shows that the electrodeposited Ta_2O_5 nanoparticles are also highly dispersed and uniform. The average size of Ta_2O_5 nanoparticles is about 50 nm. The SEM image of the CuO@Ta_2O_5 nanocomposite in Figure 1c reveals the nanoparticle size is clearly smaller than that of the electrodeposited CuO and Ta_2O_5 nanoparticles and the morphology of the surface is more homogeneous and porous. The average particle size is 45 nm.

The results of structural analysis of powders of prepared samples using XRD are presented in Figure 2. XRD pattern of CuO shows the diffraction peaks at 2θ= 32.42°, 35.65°, 38.66°, 48.84°, 53.39°, 61.64°, 66.30°and 67.97° that is consistent with the formation of monoclinic structure of CuO according to standard JCPDS card No. 48-1548 which attributing to formation (110) , (002), (111), $(20\bar{2})$, (020), $(11\bar{3})$, $(31\bar{1})$ and (220) planes, respectively [22, 23]. Figure 2b depicts the XRD pattern of Ta_2O_5 that exhibits the diffraction peaks at 2θ = 22.95◦, 28.44◦, 36.81◦, 44.97◦, 47.05◦, 49.79◦, 50.97◦,55.68◦, 58.39 and 63.71◦, corresponding to the (001), (1110), (1111), (340), (002), (0220), (2151), (1112), (2220), and (2221) planes, respectively. The result indicates the formation of the

orthorhombic phase Ta_2O_5 according to standard JCPDS card No. 25-0922 [24]. The XRD pattern of $CuO@Ta_2O_5$ nanocomposite shows the domain diffraction peaks of tetragonal $CuTa_2O_6$ at 2θ = 23.11°, 29.01° and 37.22° corresponding to (200), (211), and (310) planes, respectively, which are in agreement with standard JCPDS card No. 00-024-0380 [25]. The difference between the XRD pattern of electrodeposited CuO, Ta_2O_5 and CuO/Ta_2O_5 nanocomposite is evidence to introduction of Ta^{5+} in CuO lattice and formation of new crystal phase of tetragonal $CuTa_2O_6$ in $CuO@Ta_2O_5$ nanocomposite which will push the Cu^{2+} out of the grain [26, 27]. Therefore, tantalum will enter into grains and improve grain conductivity [26, 28].

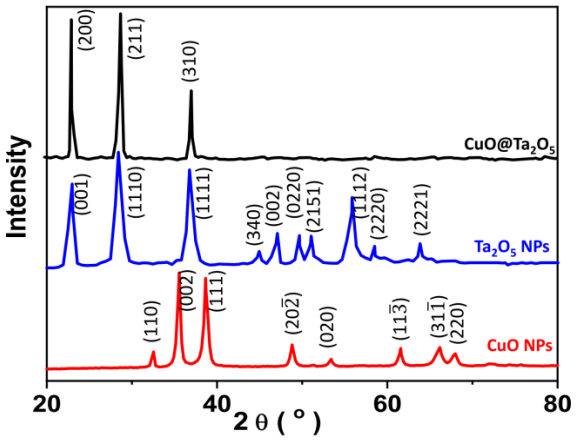

Figure 2. XRD patterns of powders of electrodeposited CuO, Ta_2O_5 and $CuO@Ta_2O_5$ nanocomposite.

3.2. Electrochemical studies of electrodeposited electrodes

The electrochemical characterization of bare GCE, and modified GCE with electrodeposited CuO NPs, Ta_2O_5 NPs and $CuO@Ta_2O_5$ nanocomposite in 0.1 M PBS pH 7.5 at scan rate of 15 mV/s are shown in Figure 3. As observed, there are not any peaks in the CV of the bare GCE. However, the CVs of CuO NPs, Ta_2O_5 NPs and $CuO@Ta_2O_5$ nanocomposite modified GCE show a small background current. After the addition of the 5 µM chrysin, the CV of the bare GCE shows a small increase in background current. The CVs of CuO NPs, Ta_2O_5 NPs and $CuO@Ta_2O_5$ nanocomposite modified GCE display one anodic peak indicating irreversible modified electrode reaction with chrysin and corresponding to the oxidation of the 5,7-dihydroxyl moiety at ring A of chrysin [29].

The CV of CuO NPs/GCE shows a shoulder like anodic peak at 0.51 V, while the CV of Ta_2O_5 NPs/GCE shows a single, broad, and obviously irreversible anodic peak at 0.47 V. The CV of $CuO@Ta_2O_5$/GCE has an anodic peak current of 0.43 V, which is three times greater than CuO NPs/GCE and two times greater than Ta_2O_5 NPs/GCE. Accordingly, the peak potential shifts to a lower potential value and the oxidation peak current is greatly enhanced at $CuO@Ta_2O_5$/GCE. According to research, morphology and surface structure play a significant role in the electrochemical response of electrodes [30, 31]. The smaller grain size and higher porosity of well-ordered porous metal oxide nanocomposite increase the effective surface area and its interaction with chrysin because

protons and electrons can diffuse into the pores and enhance electron transfer between the redox probe and the electrode surface [32, 33], which agrees with the results of SEM analysis of electrodeposited chromium. Moreover, good chemical stability and electro-catalytic activity of Ta_2O_5 NPs and CuO NPs could promote nanostructured materials' adsorption of chrysin on the modified electrode surface, and thus facilitate the electrocatalytic process of chrysin [34]. The high electrical conductivity and morphology of Ta_2O_5 and CuO enhance the easier electron transfer rate and the signal of redox reaction, which can shift the peak potential to a lower value [35, 36]. Therefore, synergistic effect of Ta_2O_5 NPs and CuO NPs in the composite enhances the catalytic sites of the modified electrodes, consequently accelerating the reaction of chrysin [37, 38].

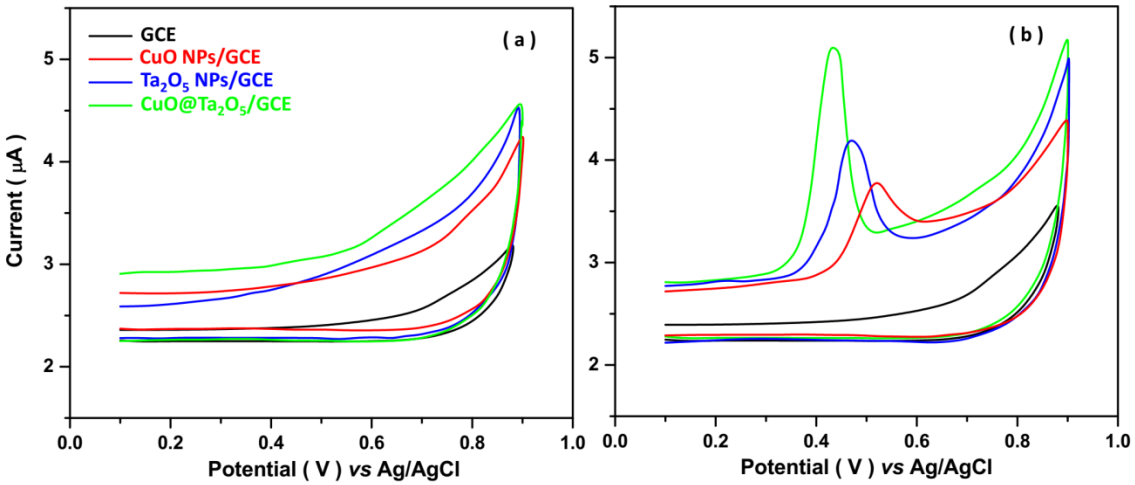

Figure 3. CV curves of bare GCE, and modified GCE with electrodeposited CuO NPs, Ta_2O_5 NPs and CuO@Ta_2O_5 nanocomposite in 0.1M PBS pH 7.5 at scan rate of 15mV/s in (a) absence of and (b) presence of 5 µM chrysin

Further studies were carried out by the amperometry technique in the investigation of modified GCE with electrodeposited CuO NPs, Ta_2O_5 NPs and CuO@Ta_2O_5 nanocomposites in response to the addition of 10 µM chrysin solutions in 0.1 M PBS pH 7.5 and a rotation speed of 1000 rpm at 0.51 V, 0.47 V and 0.43 V, respectively. Figure 4 displays the amperometric responses of all electrodes before (first 120 s) and after the addition of 10 µM chrysin solution (120 to 600s). As shown, the electrocatalytic response of CuO/GCE, Ta_2O_5/GCE and CuO@Ta_2O_5/GCE are obtained 3.17, 5.20, and 9.47 µA, respectively. In addition, the electrocatalytic signals decreased by 10, 14 and 2% for CuO/GCE, Ta_2O_5/GCE and CuO@Ta_2O_5/GCE, respectively. Moreover, the amperometric responses of Ta_2O_5/GCE and CuO@Ta_2O_5/GCE reveal a faster response to the addition of the chrysin solution than the CuO/GCE. Consequently, CuO@Ta_2O_5/GCE indicates faster, stable and stronger electrocatalytic response to the addition of 10 µM chrysin solution which related to high electrical conductivity and chemical and mechanical stability of CuO and Ta_2O_5 [24, 39]. It is suggested that an inhibited charge transfer controlled electrode reaction takes place at the Cu/Ta_2O_5 interface [40, 41].

Thus, the formation of a hetero-interface between CuO and Ta_2O_5 nanostructures can facilitate charge migration and enhance the catalytic activity of CuO@Ta_2O_5/GCE [42-44]. Therefore, the CuO@Ta_2O_5/GCE was selected for the following amperometric study for the detection of chrysin.

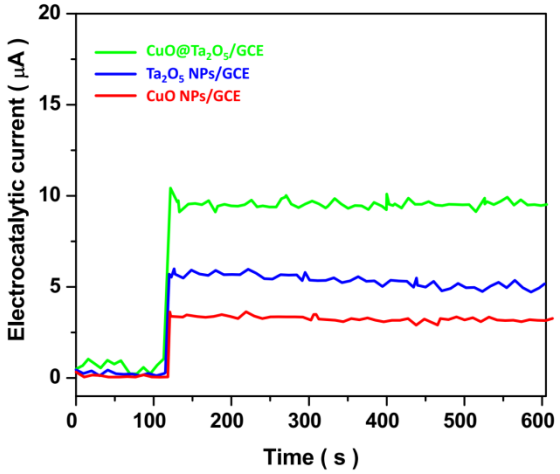

Figure 4. Amperometricresponsesof modified GCE with electrodeposited CuO NPs, Ta_2O_5 NPs and CuO@Ta_2O_5 nanocomposite to addition 10 µM chrysin solution in 0.1 M PBS pH 7.5 and rotation speed of 1000 rpm at 0.51 V, 0.47 V and 0.43 V, respectively.

Figure 5 shows the amperometric responses of CuO@Ta_2O_5/GCE to successive addition of 10µM chrysin solution in 0.1 M PBS pH 7.5 and rotation speed of 1000 rpm at 0.43 V. Figure 5a exhibits the fast response and enhancement of the electrocatalytic current step by step after the addition of each 10 µM chrysin solution. Figure 5b shows the resulting calibration plot, indicating the linear range, detection limit and sensitivity are obtained at 10 to 100 µM, 0.008 µM and 0.92921µA/µM, respectively.

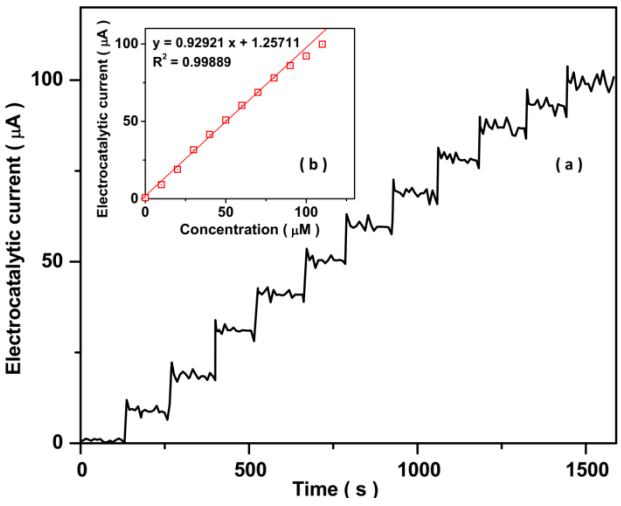

Figure 5. (a) Amperometric responses of CuO@Ta_2O_5/GCE to successive addition of 10 µM chrysin solution in 0.1 M PBS pH 7.5 and rotation speed of 1000 rpm at 0.43 V; (b) calibration plot.

Table 1 shows the comparison between the analytical parameters of the CuO@Ta_2O_5/GCE and other chrysin sensors. It is observed that the CuO@Ta_2O_5/GCE shows a wide linear range and a higher sensitivity than the other reported chrysin sensors. It can be related to the high chemical stability of CuO and Ta_2O_5 NPs, and the high density of electrochemical sites of metal oxide on the electrode surface [24, 45]. High porosity and small size of metallic nanoparticles can increase the effective area and improve electron transfer in the oxidation of chrysin [46, 47]. Furthermore, at the Cu/Ta_2O_5 interface, Cu atoms migrate into the Ta_2O_5 layer by bonding with two O atoms and Cu atoms. Cu is slightly ionized with the average charge transfer from Cu to O atom[48]. With the increase in the interface O concentration, several Ta−O−O bonding structures are formed at the interfaces which correspond to the formation of negative charges on these O ions with O−O bonds rather than those bonding with metals[48]. On the other hand, the downward bending of the band, and thus the accumulation of negative charges, should occur near the Cu/Ta_2O_5 interface which is attributed to the electrostatic interaction of CuO@Ta_2O_5 with the positively charged chrysin ions in the solution electrolyte [48, 49].

Table 1. Comparison between the analytical parameters of the CuO@Ta_2O_5/GCE and other chrysin sensors.

Electrodes	**Technique**	**detection limit (µM)**	**Linear range (µM)**	**Sensitivity (µA/µM)**	**Ref.**
CuO@Ta_2O_5/GCE	Amperometry	0.008	10-100	0.9292	This work
Ta_2O_5/chitosan/carbon paste electrode	LSV	0.03	0.08–4.0	0.8802	[11]
Activated Ta_2O_5/carbon paste electrode	LSV	0.02	0.05–7.0	0.7008	[20]
Mercury drop electrode	LSV	0.5	1-40	–	[13]
Mercury drop electrode	CV	0.1	0.37–26	–	[50]
Hypersil Gold-C18 analytical column	LC–MS/MS	0.004	0.004–2	–	[51]
ACQUITY UPLC BEH C18 column	UPLC–MS/MS	0.0004	0.0004–0.2	–	[14]

The selectivity of CuO@Ta_2O_5/GCE as a chrysin sensor was studied through an amperometric technique at 0.1 M PBS pH 7.5 and a rotation speed of 1000 rpm at 0.43 V under successive injections of 1 µM chrysin and 7 µM of other analytes as interferences. Table 2 demonstrates the significant response of the chrysin sensor to the addition of 1µM of chrysin and there are no remarkable electrocatalytic signals for the addition of other analytes. As a consequence, the CuO@Ta_2O_5/GCE did not exhibit any interfering effect with determination of chrysin in presence of the interferences which are given in Table 2, and we can consider CuO@Ta_2O_5/GCE as a selective chrysin sensor under amperometric measurements at 0.43 V.

Table 2. Results of study the interference effect of CuO@Ta_2O_5/GCE as chrysin sensor through amperometric technique in 0.1 M PBS pH 7.5 and rotation speed of 1000 rpm at 0.43 V

Analyte	**Added (µM)**	**Electrocatalytic current (µA)**	**RSD (%)**
Chrysin	1	0.91	±0.09
Ca^{2+}	7	0.08	±0.03
Cu^{2+}	7	0.10	±0.05
K^{+}	7	0.05	±0.04
Na^{+}	7	0.09	±0.02
SO_4^{2-}	7	0.06	±0.03
Zn^{2+}	7	0.08	±0.05
Folic acid	7	0.12	±0.07
Ascorbic Acid	7	0.08	±0.04
Uric Acid	7	0.09	±0.05
Citric Acid	7	0.11	±0.04
Urea	7	0.11	±0.03
Glucose	7	0.10	±0.05

The chrysin capsules were used to study the practicality of the proposed electrochemical sensor in real samples [52]. The obtained results from amperometric and HPLC measurements are presented in Table 3. The comparison reveals a good agreement between the amperometric and HPLC results. Moreover, the analytical analyses are indicated to obtain recovery (96.00% to 98.00%) and relative standard deviation (RSD) (2.77% to 3.11%) values of sample are acceptable, illustrating that CuO@Ta_2O_5/GCE can be used as a practical sensor for the detection of chrysin.

Table 3. Results of determination of chrysin in real sample using amperometric and HPLC techniques

Amperometry					HPLC	
Content in sample (µM)	Added (µM)	Measured (µM)	RSD (%)	Recovery (%)	Content in sample (µM)	RSD (%)
1.58	-	-	2.30	-	1.61	1.98
	1.00	2.54	2.77	96.00		
	2.00	3.51	2.53	96.50		
	3.00	4.49	3.07	97.00		
	4.00	5.50	3.11	98.00		

4. CONCLUSIONS

This study presented the synthesis of the CuO@Ta_2O_5 nanocomposite and enhancement of the sensing properties of CuO@Ta_2O_5 as a chrysin sensor. The nanocomposite was electrodeposited on GCE, and structural and morphological analyses showed that high porous CuO@Ta_2O_5 nanoparticles were electrodeposited on GCE. The electrochemical analyses showed the high sensitive, selective, stable and accurate response of CuO@Ta_2O_5/GCE to chrysin determination due to the synergistic effect of Ta_2O_5 NPs and CuO NPs in the composite, which enhances the catalytic sites of the modified electrodes, consequently accelerating the reaction of chrysin. The results indicated that the linear

range, detection limit and sensitivity were obtained at 10 to 100 µM, 0.008 µM and 0.92921µA/µM, respectively. The practicality of the proposed electrochemical sensor in real chrysin capsule samples was studied and the results illustrated that the obtained recovery (96.00% to 98.00%) and RSD (2.77% to 3.11%) values were acceptable. It indicates the CuO@Ta_2O_5/GCE can be used as a practical sensor to detect chrysin in pharmaceutical samples.

References

1. S. Mehdi, S. Nafees, M. Zafaryab, M. Khan and M. Alam Rizvi, *European Journal of Experimental Biology*, 8 (2018) 16.
2. X. Li, T. Shi, B. Li, X. Chen, C. Zhang, Z. Guo and Q. Zhang, *Materials & Design*, 183 (2019) 108152.
3. E. Angelopoulou, E.-S. Pyrgelis and C. Piperi, *Neurochemistry international*, 132 (2020) 104612.
4. H. Karimi-Maleh, Y. Orooji, A. Ayati, S. Qanbari, B. Tanhaei, F. Karimi, M. Alizadeh, J. Rouhi, L. Fu and M. Sillanpää, *Journal of Molecular Liquids*, 329 (2021) 115062.
5. Y. Xu, Y. Tong, J. Ying, Z. Lei, L. Wan, X. Zhu, F. Ye, P. Mao, X. Wu and R. Pan, *Oncology letters*, 15 (2018) 9117.
6. Q. Wang, S. Sun, X. Zhang, H. Liu, B. Sun and S. Guo, *Bioresource Technology*, 332 (2021) 125120.
7. L.C. Souza, M.S. Antunes, C. Borges Filho, L. Del Fabbro, M.G. de Gomes, A.T.R. Goes, F. Donato, M. Prigol, S.P. Boeira and C.R. Jesse, *Pharmacology Biochemistry and Behavior*, 134 (2015) 22.
8. Y. Zhang, G. Liu, C. Zhang, Q. Chi, T. Zhang, Y. Feng, K. Zhu, Y. Zhang, Q. Chen and D. Cao, *Chemical Engineering Journal*, 392 (2020) 123652.
9. H. Karimi-Maleh, Y. Orooji, F. Karimi, M. Alizadeh, M. Baghayeri, J. Rouhi, S. Tajik, H. Beitollahi, S. Agarwal and V.K. Gupta, *Biosensors and Bioelectronics*, 184 (2021) 113252.
10. Z. Dai, J. Xie, X. Fan, X. Ding, W. Liu, S. Zhou and X. Ren, *Chemical Engineering Journal*, 397 (2020) 125520.
11. Z. Xie, G. Li, Y. Fu, M. Sun and B. Ye, *Talanta*, 165 (2017) 553.
12. H. Karimi-Maleh, M.L. Yola, N. Atar, Y. Orooji, F. Karimi, P.S. Kumar, J. Rouhi and M. Baghayeri, *Journal of colloid and interface science*, 592 (2021) 174.
13. Z. Jian-Bin, Z. Hong-Fang and G. Hong, *Chinese Journal of Chemistry*, 23 (2005) 1042.
14. X. Zhao, X. Su, C. Liu and Y. Jia, *Molecules (Basel, Switzerland)*, 23 (2018) 1702.
15. H. Karimi-Maleh, M. Alizadeh, Y. Orooji, F. Karimi, M. Baghayeri, J. Rouhi, S. Tajik, H. Beitollahi, S. Agarwal and V.K. Gupta, *Industrial & Engineering Chemistry Research*, 60 (2021) 816.
16. Z. Savari, S. Soltanian, A. Noorbakhsh, A. Salimi, M. Najafi and P. Servati, *Sensors and Actuators B: Chemical*, 176 (2013) 335.
17. H. Karimi-Maleh, S. Ranjbari, B. Tanhaei, A. Ayati, Y. Orooji, M. Alizadeh, F. Karimi, S. Salmanpour, J. Rouhi and M. Sillanpää, *Environmental Research*, 195 (2021) 110809.
18. J.-B. Liu, M. Ren, X. Lai and G. Qiu, *Chemical Communications*, 57 (2021) 4259.
19. Y. Duan, Y. Liu, Z. Chen, D. Liu, E. Yu, X. Zhang, H. Fu, J. Fu, J. Zhang and H. Du, *Green Chemistry*, 22 (2020) 44.
20. Z. Xie, Y. Wu, S. Kai, G. Li and B. Ye, *Electroanalysis*, 29 (2017) 835.
21. P. Arul and S.A. John, *Journal of Electroanalytical Chemistry*, 799 (2017) 61.
22. H. Xu, W. Wang, W. Zhu, L. Zhou and M. Ruan, *Crystal Growth and Design*, 7 (2007) 2720.

23. D. Zhu, L. Wang, W. Yu and H. Xie, *scientific reports*, 8 (2018) 1.
24. F. Magesa, Y. Wu, S. Dong, Y. Tian, G. Li, J.M. Vianney, J. Buza, J. Liu and Q. He, *Biomolecules*, 10 (2020) 110.
25. P. Ndalamba and M. Sundberg, *Materials Research Bulletin - MATER RES BULL*, 19 (1984) 807.
26. K. Miura, T. Osawa, Y. Yokota, Z. Hossain and O. Hanaizumi, *Journal of Materials Science and Chemical Engineering*, 3 (2015) 47.
27. H. Savaloni and R. Savari, *Materials Chemistry and Physics*, 214 (2018) 402.
28. Y. Yang, H. Chen, X. Zou, X.-L. Shi, W.-D. Liu, L. Feng, G. Suo, X. Hou, X. Ye and L. Zhang, *ACS applied materials & interfaces*, 12 (2020) 24845.
29. P. Janeiro, O. Corduneanu and A.M. Oliveira Brett, *Electroanalysis: An International Journal Devoted to Fundamental and Practical Aspects of Electroanalysis*, 17 (2005) 1059.
30. L. Wang, Y. Liu and Y. Chen, *International Journal of Electrochemical Science*, 16 (2021) 210464.
31. F. Dong, L. Zhang, R. Li, Z. Qu, X. Zou and S. Jia, *International Journal of Electrochemical Science*, 16 (2021) 210234.
32. Y. Wang, H. Arandiyan, J. Scott, A. Bagheri, H. Dai and R. Amal, *Journal of Materials Chemistry A*, 5 (2017) 8825.
33. H. Savaloni, R. Savari and S. Abbasi, *Current Applied Physics*, 18 (2018) 869.
34. S. Zhou, Z. Deng, Z. Wu, M. Xie, Y. Tian, Y. Wu, J. Liu, G. Li and Q. He, *Nanomaterials (Basel, Switzerland)*, 9 (2019) 811.
35. K.Y. Hwa, P. Karuppaiah, N. Gowthaman, V. Balakumar, S. Shankar and H.N. Lim, *Ultrasonics sonochemistry*, 58 (2019) 104649.
36. L. Tan, Y. Sun, C. Wei, Y. Tao, Y. Tian, Y. An, Y. Zhang, S. Xiong and J. Feng, *Small*, 17 (2021) 2007717.
37. S. Phetsang, P. Kidkhunthod, N. Chanlek, J. Jakmunee, P. Mungkornasawakul and K. Ounnunkad, *Scientific reports*, 11 (2021) 1.
38. Y. Jiang, P. Liu, Y. Liu, X. Liu, F. Li, L. Ni, Y. Yan and P. Huo, *Separation and Purification Technology*, 170 (2016)
39. Z. Yang, P. Xu, W. Wei, G. Gao, N. Zhou and G. Wu, *IEEE Transactions on Plasma Science*, 48 (2020) 2822.
40. T. Tsuruoka, I. Valov, S. Tappertzhofen, J. van den Hurk, T. Hasegawa, R. Waser and M. Aono, *Advanced functional materials*, 25 (2015) 6374.
41. Z. Hou, H. Lu, Y. Li, L. Yang and Y. Gao, *Frontiers in Materials*, 8 (2021) 91.
42. Y. Su, H. Guo, Z. Wang, Y. Long, W. Li and Y. Tu, *Sensors and Actuators B: Chemical*, 255 (2018)
43. K. Yang, Q. Liu, Y. Zheng, H. Yin, S. Zhang and Y. Tang, *Angewandte Chemie*, 133 (2021) 6396.
44. Y. Liu, T. Xu, Y. Liu, Y. Gao and C. Di, *Journal of Materials Research and Technology*, 9 (2020) 8283.
45. W. Xu, S. Dai, X. Wang, X. He, M. Wang, Y. Xi and C. Hu, *Journal of Materials Chemistry B*, 3 (2015) 5777.
46. E. Fazio, S. Spadaro, C. Corsaro, G. Neri, S.G. Leonardi, F. Neri, N. Lavanya, C. Sekar, N. Donato and G. Neri, *Sensors*, 21 (2021) 2494.
47. H. Savaloni, E. Khani, R. Savari, F. Chahshouri and F. Placido, *Applied Physics A*, 127 (2021) 1.
48. B. Xiao and S. Watanabe, *ACS applied materials & interfaces*, 7 (2015) 519.
49. D.S.R. Josephine, K.J. Babu and K. Sethuraman, *Microchimica Acta*, 184 (2017) 781.
50. N. Sun, W.-m. Mo, B.-x. Hu and Z.-l. Shen, *Physical Testing and Chemical Analysis Part B Chemical Analysis*, 9 (2005) 41.

51. L. Tong, M. Wan, L. Zhang, Y. Zhu, H. Sun and K. Bi, *Journal of pharmaceutical and biomedical analysis*, 70 (2012) 6.
52. Q. Hu, W. Zhang, Q. Yin, Y. Wang and H. Wang, *Spectrochimica Acta Part A: Molecular and Biomolecular Spectroscopy*, 244 (2021) 118864.